

## ANALYSIS OF THE MIGDAL TRANSFORMATION FOR MODELS WITH PLANAR SPINS ON A TWO-DIMENSIONAL LATTICE

K. SOKALSKI

*Uniwersytet Jagielloński, Kraków, Poland\**

Th.W. RUIJGROK and B. SCHOENMAKER

*Rijksuniversiteit, Utrecht, The Netherlands\*\**

Received 12 February 1987

By numerical and analytical investigations we show that the bond-moving transformation of Migdal for planar spins on a two-dimensional lattice possesses a very rich structure. We find an infinite hierarchy of one-, three- and higher-dimensional fixed spaces. In addition to phase transitions of the Kosterlitz–Thouless-type, we find Ising-like transitions, for which the critical exponents are the same as those of the  $q$ -state Potts model in the Migdal approximation. These critical exponents are constant within each fixed space. The phase diagram is constructed for two specially chosen potentials.

### 1. Introduction

The system under consideration consists of a square lattice with a two-dimensional continuous spin-vector of unit length at every site and with an isotropic nearest neighbour interaction of the general form

$$-\beta H = \sum_{(i,j)_{n.n.}} h(\mathbf{S}_i \cdot \mathbf{S}_j). \quad (1.1)$$

Special cases of these so-called  $XY$ -interactions include for the  $XY$ -model in the strict sense

$$h(u) = Ku \quad (1.2)$$

\*Mailing address: Instytut Fizyki, Reymonta 4, 30-059, Kraków, Poland.

\*\*Mailing address: Instituut voor Theoretische Fysica, Princetonplein 5, P.O. Box. 80.006, 3508 TA Utrecht, The Netherlands.

and

$$h(u) = Ku^2 \quad \text{for the Maier-Saupe model,} \quad (1.3)$$

where  $u = S_i \cdot S_j = \cos \varphi_{ij}$ . Combinations of these interactions have recently been shown<sup>1,2</sup>) to describe systems exhibiting more than one phase transition. Since this increase in the number of phases occurs when a two-parameter instead of a one-parameter Hamiltonian is considered, it is to be expected that an enormous proliferation will take place when arbitrary interaction functions  $h(u)$  are admitted. So far the exact treatment of this problem is out of the question. If it is admitted, however, that the bond-moving method à la Migdal<sup>3</sup>) does not introduce a complete distortion of the essential features of the system, it becomes possible to study all possible phase transitions in very great detail. The beginning of such an investigation was given in a previous publication<sup>4</sup>), in which the Migdal renormalization was applied to two- and three-dimensional lattices carrying two- or three-dimensional spins on their sites. For the three-dimensional lattice with three-dimensional spins we indeed found a number of relevant fixed points of the Migdal transformation, one of which indicated the existence of a new so-called antinematic phase. However, a full discussion of the case of two-dimensional spins on a square lattice was not given there. It is the purpose of this paper to remedy this situation and to exhibit the rich phase structure of this simple system.

We begin by recalling the renormalization group equations obtained by the bond-moving approximation of Migdal. In the form derived in ref. 4 they read

$$\exp[g_m + h_{m+1}(S_1 \cdot S_2)] = \int dS \exp[2\{h_m(S_1 \cdot S) + h_m(S_2 \cdot S)\}], \quad (1.4)$$

$$e^{g_m} = e^{-\bar{h}} \int dS \exp[4h_m(S_1 \cdot S)], \quad (1.5)$$

with

$$h_{m+1}(1) = h_m(1) = \bar{h} \quad \text{and} \quad h_0(u) = h(u). \quad (1.6)$$

For the iteration process it is more convenient to use a discrete representation of the functions  $h_m(\cos \varphi)$ , by writing

$$e^{-2V(\varphi)} = \mu_0 + 2 \sum_{l=1}^{\infty} \mu_l \cos l\varphi, \quad (1.7)$$

where

$$V(\varphi) = \bar{h} - h_m(\cos \varphi) \quad \text{and} \quad V(0) = 0. \quad (1.8)$$

Defining  $\mu_{-l} \equiv \mu_l$ , eq. (1.7) takes the form

$$e^{-2V(\varphi)} = \sum_{l=-\infty}^{\infty} \mu_l \cos l\varphi. \quad (1.9)$$

From eq. (1.8) we see that

$$\sum_{l=-\infty}^{\infty} \mu_l = 1. \quad (1.10)$$

The Migdal transformation (1.4), (1.5) now becomes

$$\mu'_l = \frac{1}{D^2} \sum_m \mu_m^2 \mu_{m+l}^2 \quad \text{with} \quad D = \sum_m \mu_m^2. \quad (1.11)$$

Notice that  $\sum_l \mu'_l = 1$ , even if  $\sum_l \mu_l \neq 1$ , but that  $\mu'_{-l} = \mu'_l$  only holds if also  $\mu_m$  is symmetric.

The numerical and analytical investigation of eq. (1.11) is the main subject of the present paper. Before embarking on this, however, we want to make some preliminary remarks.

Firstly we observe<sup>4)</sup> that if  $F = \{\mu_l\}$  is a fixed point of the mapping (1.11), or an almost fixed point in a sense to be explained later, also the point  $F(p) = \{\tilde{\mu}_l\}$  with

$$\tilde{\mu}_l = \begin{cases} \mu_{l/p} & \text{if } l/p \text{ integer,} \\ 0 & \text{otherwise} \end{cases} \quad (1.12)$$

is an (almost) fixed point. The corresponding potential is  $\tilde{V}(\varphi) = V(p\varphi)$ . An exact fixed point is given by the trivial solution T, for which  $\mu_l = \delta_{l0}$ . In this case the corresponding potential is  $V_T(\varphi) = 0$ , which describes the high temperature phase in which the spin-interactions play no role anymore. Ito<sup>5)</sup> has shown that within a certain class of potentials  $V(\varphi)$  this  $V_T(\varphi)$  is the only exact fixed point of the mapping (1.11).

A set of almost fixed points is given by the line of Gaussian points  $G(0) = \{\mu_l\}$ , with

$$\mu_l = \mu_0 e^{-bl^2} \quad (b > 0 \text{ arbitrary}). \quad (1.13)$$

From eq. (1.10) we get the relation between  $\mu_0$  and  $b$ :

$$\mu_0^{-1} = \sum_l e^{-bl^2}. \quad (1.14)$$

For  $b \ll 1$  the summation may be replaced by an integration and we get

$$\mu_0 \approx \sqrt{\frac{b}{\pi}} \quad \text{for } b \rightarrow 0. \quad (1.15)$$

On substituting (1.13) into the mapping (1.11) and transforming the summations with the help of Poisson's formula, we obtain

$$\mu'_l = \mu_l (1 \pm 2 e^{-\pi^2/4b} + \dots), \quad (1.16)$$

where the plus and minus signs must be taken for even and odd  $l$ -values, respectively. The Gaussian line, therefore, does not consist of exact fixed points, but for small  $b$  the approximation is extremely good. For  $\chi^2 \equiv \sum_l (\mu'_l - \mu_l)^2$  we find

$$\chi^2 = 2e^{-\pi^2/2b}. \quad (1.17)$$

We have tried to find really fixed points in the neighbourhood of such a Gaussian point by numerically minimising  $\chi^2$  with respect to  $\{\mu_l\}$ . In fig. 1 the value of this minimum  $\chi^2$  is plotted as a function of  $1/\mu_0^2 \approx \pi/b$ . The

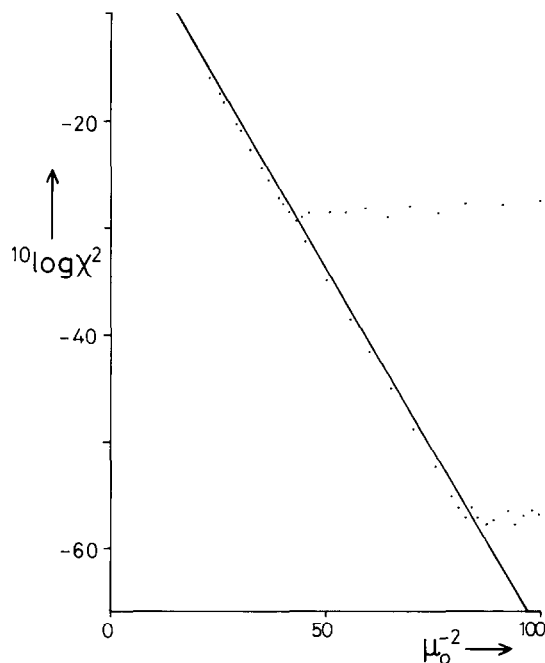


Fig. 1.  $\chi^2$  for the numerically found almost fixed line close to the Gaussian line, in single and double precision, as a function of  $1/\mu_0^2$ .

calculations were done in single as well as in double precision. It is seen that only a slight improvement is made over the value as given by eq. (1.17), but that no exact fixed points are found. The flattening of the curves is explained by the  $\mu'_l$  and  $\mu_l$  becoming equal within the computer accuracy. Our calculations confirm the results of José et al.<sup>6)</sup> and extend them to higher precision. The Gaussian line of almost fixed points therefore has no well-defined end point  $b_{cr}$  in the parameter  $b$ . Such an end point is essential for the existence of the Kosterlitz–Thouless (KT) transition. It has disappeared<sup>7)</sup> in the Migdal approximation, but can be recovered in an artificial way in numerical calculations by setting  $\chi^2$  in eq. (1.17) equal to the square of the computer accuracy, i.e.  $10^{-28}$  in single precision. Taking for  $b_{cr}$  the corresponding  $b$ -value, i.e.  $b_{cr} = 0.075$ , then, for all practical purposes, the Gaussian points with  $b < b_{cr}$  cannot be distinguished from exact fixed points. Although the numerical values for thermodynamic quantities and the position of the KT transition obtained in this way cannot be expected to be very realistic, the phase diagram is probably not very much distorted.

The behaviour of the mapping in the neighbourhood of a fixed point is characterised by the eigenvalues of the linearised mapping. For the trivial fixed point T these eigenvalues are all equal to zero. For every point of the Gaussian line the spectrum was numerically found to be<sup>4)</sup>

$$\lambda_k = \left(\frac{1}{4}\right)^k, \quad k = 0, 1, 2, \dots \quad \text{for all } b \ll 1, \quad (1.18)$$

where these values are accurate to within more than ten decimal places. This regularity and independence of  $b$  will be explained in section 3. If the largest eigenvalue  $\lambda_0$  were exactly equal to unity this would indicate the existence of a line of fixed points. This follows from the fact that if  $\mu_l(b)$  is a fixed point of the mapping  $\mu_l = T_l\{\mu\}$  in a range of  $b$ -values, then  $d\mu_l/db = \Sigma_j (\partial T_l / \partial \mu_j) (d\mu_j/db)$ , so that  $d\mu_l/db$  is an eigenvector of the linearised mapping with eigenvalue  $\lambda_0 = 1$ .

We see that in the limit  $b \rightarrow 0$  the corresponding point of G(0) becomes an exact fixed point, but with a spectrum which is different from that of T. In this limit it gives a singular potential which falls outside the class of functions considered by Ito<sup>5)</sup>. Using eq. (1.19) and applying again Poisson's summation formula we obtain

$$e^{-2V_G(\varphi)} = \sqrt{\frac{\pi}{b}} \sum_m e^{-(\varphi - 2\pi m)^2 / 4b} \quad \text{for } b \ll 1. \quad (1.19)$$

This gives the potential used by Villain<sup>8)</sup> in a model which is a generalisation of the XY-model in the strict sense<sup>9)</sup>. In the same sense the fixed points G( $p$ )

correspond with the potential  $V_G(p\varphi)$ , which is the Villain potential with fractional charges.

Another line of almost fixed points was found numerically and could excellently be fitted by

$$\mu_{2l} = \mu_0 e^{-b(2l)^2}; \quad \mu_{2l+1} = a\mu_0 e^{-b(2l+1)^2}; \quad a = 0.543689. \quad (1.20)$$

For small  $b$  this is indeed a fixed point of the mapping (1.11), provided that the constant  $a$  be a solution of

$$a^4 - 2a + 1 = 0. \quad (1.21)$$

The value of eq. (1.20) indeed satisfies this equation. In this way we have found a new line of (almost) fixed points, which we will call  $RG_2(0)$ , because it is an extension of the Gaussian line consisting of 2 subseries and with one relevant (R) eigenvalue  $\lambda_{\max} > 1$  of the linearised mapping. In fact we found by numerical calculation that there is a double series of eigenvalues, independent of  $b$  and given by

$$\lambda_k^{(1)} = \left(\frac{1}{4}\right)^k \lambda_{\max} \quad \text{and} \quad \lambda_k^{(2)} = \left(\frac{1}{4}\right)^k, \quad k = 0, 1, 2, \dots \text{ for } RG_2(0) \quad (1.22)$$

with

$$\lambda_{\max} = 1.6785736 \dots$$

The analytical calculation of these series will again be given in section 3. As was shown in eq. (1.12) also here we can construct relevant fixed points  $RG_2(p)$  with higher periodicity for the corresponding potential.

Since  $\lambda_{\max} > 1$  an initial point  $\{\mu_l\}$  slightly off  $RG_2(0)$  will map away from it. It turns out (numerically) that it is attracted either by  $G(0)$  or by  $G(1)$ . By considering the basins of attraction of T,  $G(0)$  and  $G(1)$  we therefore get a structure as shown schematically in fig. 2. The dashed line through the end points of the lines of (almost) fixed points represents the Kosterlitz–Thouless transition, whereas  $RG_2(0)$  is the separatrix across which an Ising-like transition takes place. The latter does not depend on where we put the end points of the fixed lines. In principle the flow as shown in fig. 2 takes place in the infinite-dimensional  $\mu$ -space. It turns out, however, that when the starting point of the mapping is taken to be of the form of eq. (1.20) with  $0 < a < 1$  and  $b \ll 1$ , the application of the mapping results in a point which, to a very good approximation, is again of the same form. The value of  $a$  is changed, but  $b$  is

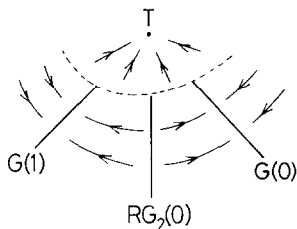


Fig. 2. Schematic diagram of a small part of the (infinite-dimensional) flow diagram.

not altered. For larger values of  $b$  this approximation of the full mapping by a mapping in a two-dimensional space  $(a, b)$  deteriorates, until for  $b \geq b_{cr}$  it completely fails. A point of the form (1.20) then very quickly maps into the trivial point  $T$ . This behavior is shown in fig. 3, where it should be remembered that the dashed lines do not really lie in the  $(a, b)$  plane. In a recent paper<sup>2)</sup> Korshunov also considers initial points of the form (1.20) (His  $f_1$  is our  $a$  and his  $J$  is equal to  $2b$  in our case). He then proceeds to change the Migdal transformation in such a way that the mapping becomes exactly two-dimensional:  $(a, b) \rightarrow (a', b')$ . This he calls the one-charge approximation. By doing so he loses the possibility for a point to map into the trivial point  $T$ . For small  $b$  his fig. 4 is identical to our fig. 3. For larger  $b$ -values, however, he finds that the two fixed lines  $G(0)$  and  $RG_2(0)$  meet in the point  $a = (\frac{1}{3})^{1/4} = 0.75983$ ,  $b = 0.72$ . From fig. 3 it is seen, however, that this meeting point lies in the region where the initial point maps into  $T$ . Therefore the one-charge approximation is correct for small  $b$ -values, but gives spurious results for  $b \geq 0.1$ .

The fixed points of eq. (1.11) mentioned up to now far from exhaust the list of all fixed points. We have found many more, which we will describe and try to classify in the next section. In section 3 we will introduce a continuum

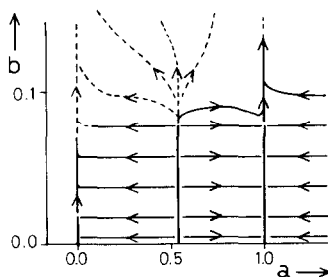


Fig. 3. An approximate two-dimensional flow diagram for points of the form (1.20). Full lines lie in the  $a$ - $b$  plane to a very good approximation, dashed lines are the projections of trajectories leaving this plane. The thick vertical lines at  $a = 0.0, 0.543, \dots, 1.0$  are the almost fixed lines  $G(1)$ ,  $RG_2(0)$  and  $G(0)$ .

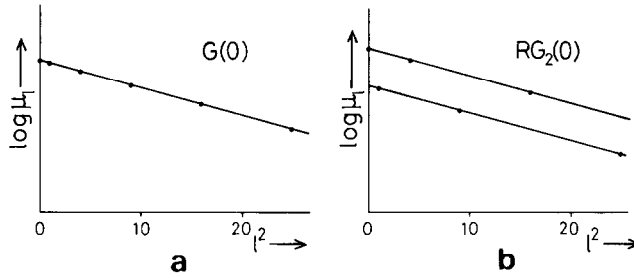


Fig. 4. (a) One- and (b) two-line solutions, (1.13) and (1.20), in the logarithmic scale.

approximation, which will allow us to exactly determine the structure of the fixed points described in section 2, as well as to calculate the full spectrum of the linearised mapping in such a point. The potentials corresponding to these fixed points are calculated and plotted in section 4. There we also show the phase diagrams for a number of interactions, which recently were discussed in the literature. A resume of our results is given in section 5.

## 2. Classification of fixed points

When plotting  $\log \mu_i$  versus  $l^2$  for the solutions  $G(0)$  of eq. (1.13) and  $RG_2(0)$  of eq. (1.20) we obtain one and two straight lines as shown in figs. 4a and 4b. This suggests that other relevant fixed points can be found by putting the points  $\mu_i$  on three or more parallel lines. By taking this as an ansatz and varying the distances between the lines we indeed found solutions for which  $\chi^2 = \sum_i (\mu'_i - \mu_i)^2$  was as small as the computer accuracy of  $10^{-28}$ . We will denote them by  $RG_n(0)$ , where  $n$  is the number of parallel lines. Like for the Gaussian points  $G(0)$ , the slope of these lines,  $-b$ , is a free parameter and again for each  $b < b_{cr} \approx 0.075$ , the point  $RG_n(0)$  is an exact fixed point to within the numerical accuracy.

In order to linearise a mapping  $\mu'_i = T_i(\mu)$  in a fixed point  $\mu_i^*$ , one writes  $\mu_i = \mu_i^* + v_i$  and  $\mu'_i = \mu_i^* + v'_i$ , where  $v_i$  and  $v'_i$  are infinitesimally small. The mapping becomes

$$v'_i = M_{ij} v_j, \quad (2.1)$$

(with the summation convention) where  $M_{ij} = (\partial T_i / \partial \mu_j)_{\mu^*}$ . In the present case

$$M_{ij} = \frac{2\mu_j^*}{D^2} (\mu_{j+1}^{*2} - 2D\mu_i^* + \mu_{j-1}^{*2}). \quad (2.2)$$



For  $G(0)$ , as was remarked before,  $\lambda = 1$  is very close to an eigenvalue of this matrix at least for small  $b$ . It turns out also to be the largest eigenvalue, so that the whole line  $G(0)$  is an attractor. For the (almost) fixed lines  $RG_n(0)$ , however, we find that the largest eigenvalue of  $M$  is greater than one. Like for the special case of  $RG_2(0)$ , cf. eq. (1.22), we also find by numerical calculation that with every eigenvalue  $\lambda$  also  $\lambda/4$  is an eigenvalue of  $M$ . It is not difficult to prove (and verify numerically) that the spectrum of  $M$  for a fixed point  $F(p)$ , as defined by eq. (1.12), is the same as for  $F(0)$ .

In table I and table II we give the line structure of all fixed points  $RG_n(0)$  for  $n = 1$ , i.e.,  $G(0)$ ,  $n = 2$  and  $n = 3$ , together with the relevant eigenvalues of the corresponding  $M$ . For later use also the distances between the lines were determined with a five decimal accuracy. They are, however, not reported here. Notice that for fixed  $j$  ( $0, 1, 2, \dots, n-1$ ) all points  $\mu_{nl+j}$  and  $\mu_{nl-j}$  ( $l = 0, 1, 2, \dots$ ) lie on the same line. This symmetry, which is a direct consequence of the mapping, is used to fix the number of lines, even if some of them coalesce.

Using the analysis of the next section we have shown that for  $n = 1, 2, 3$  and 4 the lines of fixed points  $RG_n(0)$  are exhausted by those given in table I and table II. For larger values of  $n$  we only give a few examples in table III. Since in these examples the largest eigenvalue is larger than two, the value of the specific heat goes to infinity in the corresponding phase transition. Whether or not this is an artefact of the Migdal approximation cannot be decided in the present framework. The largest eigenvalues were found for the most degenerate structure  $RG_{N+1}^{(d)}(0)$ , in which  $N$  lines coincide. The results fully agree with the analysis of this case as given in the next section. (See table IV.) We also found one-dimensional spaces of fixed points with a mixed character as shown in fig. 5. They will not be investigated any further. A more interesting class of

TABLE I  
All one-, two- and three-line solutions with their relevant eigenvalues.

Name	Structure	$\lambda \geq 1$
$G(0)$	o---o---o---o---o-	1.0
$RG_2(0)$	o-----o-----o---	1.678573
	----o-----o-----	1.0
$RG_3^{(1)}(0)$	o-----o---	1.678571
	----o-----o-----	1.0
	-----o-----	
$RG_3^{(2)}(0)$	o-----o---	1.852602
	----o---o---o---	1.277792
		1.0

TABLE II  
All four-line solutions with their relevant eigenvalues.

Name	Structure	$\lambda \geq 1$
$RG_4^{(1)}(0)$	o-----o--	1.122613
	---o-----o---	1.0
	-----o--o-----	
	-----o-----	
$RG_4^{(2)}(0)$	o-----o--	1.895972
	---o--o-----o--o---	1.417297
	-----o-----	1.0
$RG_4^{(3)}(0)$	o-----o-----o--	1.777777
	---o--o-----o--o---	1.0
$RG_4^{(4)}(0)$	o-----o--	1.963480
	--o--o--o--o--o--o---	1.197514 (2 $\times$ )
		1.0
$RG_4^{(5)}(0)$	o-----o--	1.777777
	-----o-----	1.678571
	---o-----o-----	1.0
	--o-----o-----	
$RG_4^{(6)}(0)$	o-----o--	1.89597
	---o-----o-----	1.41729
	-----o--o-----	1.0

TABLE III  
Some five-line solutions with their relevant eigenvalues.

Name	Structure	$\lambda \geq 1$
$RG_5^{(1)}(0)$	-o-----o	2.015208
	---o-----o---	1.301311
	--o-----o--	1.0
	-----o--o-----	
	-----o-----	
$RG_5^{(2)}(0)$	o-----o--	2.045356
		1.139680 (3 $\times$ )
	-o-o-o-o-o-o-o-o---	1.0

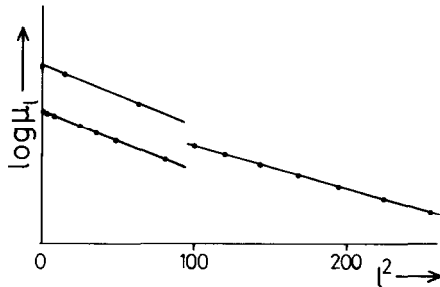


Fig. 5. A mixed solution, consisting of two earlier found solutions.

(almost) fixed points, which we also found by numerical methods, will be denoted by  $SG(p)$ .

In order to study the mapping (1.11) numerically, it was necessary to restrict the number of terms in this equation. The special solution just mentioned above was found only when this cut off was not smaller than about one hundred. The G stands for Gaussian, indicating the overall Gaussian nature of  $\mu_l$  and for the fact that the largest eigenvalue is equal to one. The S, for special structure, is meant to describe not only the modification of  $\mu_l$ , but also the fact that the eigenvalue  $\lambda = 1$  is three-fold degenerate. The index  $p$  plays a similar role as in  $G(p)$ .

The three-fold degeneracy of  $\lambda = 1$  is explained by the fact that there is a three-dimensional subset of the infinite-dimensional parameter space containing only (almost) fixed points. The eigenvalues of  $M$  are again the same in each point of this subset. An excellent fit of such an  $SG(p)$  point is given by

$$\mu_l = \bar{\mu} \sum_{i=-\infty}^{+\infty} e^{-\gamma i^2} \cdot e^{-b(l-\alpha i)^2}, \quad (2.3)$$

where  $\bar{\mu} = \sqrt{b\gamma}/\pi$  is the normalisation constant, determined by  $\sum_l \mu_l = 1$ . There are indeed three independent continuous parameters  $\alpha$ ,  $b$  and  $\gamma$ , although  $\alpha$  is not allowed to lie too close to an integer value. A typical example is obtained by taking  $\alpha = 10.3$ ,  $b = 0.25$ ,  $\gamma = 0.07$ . A relevant counterpart  $SR_2(p)$  of these special points was also found. It could be parametrised by

$$\mu_l = \bar{\mu} \sum_{i=-\infty}^{+\infty} [e^{-\gamma(2i)^2} e^{-b(l-2i\alpha)^2} + a e^{-\gamma(2i+1)^2} e^{-b(l-(2i+1)\alpha)^2}], \quad (2.4)$$

where  $a = 0.543689$  has again the same value as in eq. (1.20). The continuum analysis of these three-dimensional structures will again be given in section 3. From this it will then become apparent that also higher-dimensional spaces of fixed points exist. Some classification will be given in section 5.

### 3. The continuum limit

In all numerical calculations we have used the mapping of eq. (1.11), which we now write as

$$I: \quad u'_l = \frac{1}{D^2} \sum_m u_m^2 u_{m+l}^2 \quad \text{with} \quad D = \sum_m u_m^2. \quad (3.1)$$

Only symmetric functions  $u_{-l} = u_l$  are allowed. For analytical purposes, how-

ever, it is more convenient to consider the mapping

$$\text{II:} \quad z'_l = \sum_m z_m^2 z_{m+l}^2 \quad \text{with} \quad z_{-l} = z_l. \quad (3.2)$$

The relation between the fixed points of I and II is given by

$$u_l^* = \frac{1}{\alpha^{*2}} z_l^*, \quad (3.3)$$

where  $\alpha^*$ , defined by

$$\alpha^* \equiv \sum_l z_l^{*2}, \quad \text{satisfies} \quad \sum_l z_l^* = \alpha^{*2}. \quad (3.4)$$

Also the spectra of I and II are simply related. The matrix of the linearised mapping of I, i.e. eq. (2.2), can be written as

$$M_{lj} = 2z_j^*(z_{j+l}^{*2} + z_{j-l}^{*2}) - \frac{4}{\alpha^*} z_l^* z_j^* \equiv \tilde{M}_{lj} - \frac{4}{\alpha^*} z_l^* z_j^*, \quad (3.5)$$

in which  $\tilde{M}_{lj}$  is the matrix for the linearisation of II in the same fixed point. The vector  $\tilde{e}_0 = \tilde{z}^*$  is an eigenvector of  $\tilde{M}$  with eigenvalue  $\lambda = 4$ . It is also an eigenvector of  $M$ , but with eigenvalue zero. All other eigenvalues of  $M$  are equal to those of  $\tilde{M}$ . The reader can easily convince himself of this fact by checking that the eigenvectors are related as follows:

$$e_n = \tilde{e}_n - \frac{4}{\alpha^* \lambda_n} (z^* \cdot \tilde{e}_n) z^*. \quad (3.6)$$

Therefore only the eigenvalue  $\lambda = 4$  has to be omitted from the spectrum of  $\tilde{M}$  in order to obtain the spectrum of  $M$ .

The potential  $V^*(\varphi)$  belonging to a fixed point is given by eq. (1.9), which now becomes

$$e^{-2V^*(\varphi)} = \frac{1}{\alpha^{*2}} \sum_l z_l^* \cos l\varphi. \quad (3.7)$$

Using the equation for the fixed point this can be shown to be positive and not greater than one. The potential for the fixed point is therefore real, as it should, but nowhere less than the value  $V^*(\varphi = 0) = 0$ .

A functional  $\phi[z]$  which is useful in studying the mapping II is given by

$$\phi[z] = -2 \sum_m z_m^3 + \sum_{k,m} z_k^2 z_{k+m}^2 z_m^2. \quad (3.8)$$

For a point in the symmetric space  $z_{-j} = z_j$ , its gradient is given by

$$\frac{\partial \phi}{\partial z_l} = 6z_l(z'_l - z_l), \quad (3.9)$$

so that the fixed points of II coincide with the points where  $\phi[z]$  is stationary.

We now introduce the continuum approximation of II by replacing  $z_m$  by the even function  $z(x)$ . Then the mapping becomes

$$z'(y) = \int_{-\infty}^{\infty} dx z^2(x) z^2(x+y), \quad z(-x) = z(x). \quad (3.10)$$

An exact fixed point of this equation is the Gaussian line

$$G(0): \quad z(x) = z_0 e^{-bx^2} \quad \text{with} \quad z_0^3 = \sqrt{\frac{4b}{\pi}} \quad \text{for all } b > 0. \quad (3.11)$$

Later in this section we will return to this solution, but first we want to remark that the form of eq. (3.10) is invariant under the scaling transformation

$$z(x) \rightarrow \tilde{z}(x) = \alpha^{1/3} z(\alpha x). \quad (3.12)$$

From this we find the scale invariant fixed point

$$z(x) = \frac{q}{|x|^{1/3}} \quad \text{with} \quad q^{-3} = \int_{-\infty}^{\infty} \frac{du}{|u|^{2/3} \cdot |u-1|^{2/3}}. \quad (3.13)$$

The integral can be calculated and gives  $q = (2\pi)^{1/3} / [\sqrt{3}\Gamma(1/3)] = 0.39768 \dots$ . The quantity  $\alpha^{*2}$ , occurring in eq. (3.7), however diverges for this solution. Therefore  $V^*(\varphi = 0)$  cannot be made to vanish. It is possible, however, to normalise the potential in such a way that it vanishes at  $\varphi = \pm \pi$ .

Instead of (1.5) and (1.6) we now have

$$h_{n+1}(-1) = h_n(-1) = \bar{h}, \quad (3.14)$$

$$\exp(g_n) = \exp(-\bar{h}) \cdot \int dS \exp[2\{h_n(S_1 \cdot S) + h_n(-S_1 \cdot S)\}].$$

The mapping (1.11) becomes (with the same expansions (1.8) and (1.9)):

$$\mu'_l = \frac{1}{D_1^2} \sum_m \mu_m^2 \mu_{m+l}^2 \quad \text{with} \quad D_1 = \sum_m \mu_{2m}^2 - \sum_m \mu_{m+1}^2. \quad (3.15)$$

Only the normalisation factor has changed. The  $\mu_l$  now satisfy

$$\sum_l (-1)^l \mu_l = 1. \quad (3.16)$$

The quantity  $D_1$  stays finite if we discretize (3.13):

$$\mu_l = \begin{cases} q_1 |l|^{-1/3}, & l \neq 0, \\ \mu_0, & l = 0. \end{cases} \quad (3.17)$$

It is not possible to choose  $q_1$  and  $\mu$  in such a way that  $\mu_l$  is an exact fixed point of the mapping. If we choose  $q_1 = 0.836 \dots$  and  $\mu_0 = 1.985 \dots$ , the relation  $\mu'_l = \mu_l$  holds for  $l = 0$  and in the limit  $l \rightarrow \infty$ . The normalisation, however, is not satisfied in this case:

$$\mu_0 + 2q_1 \sum_{l=1}^{+\infty} (-1)^l |l|^{-1/3} \approx 1.028 \neq 1. \quad (3.18)$$

It was not possible to search numerically for an exact solution in the neighbourhood of this approximate one, because for  $l \rightarrow \infty$  the  $\mu_l$  approach zero extremely slowly and the cut-off number of  $\mu_l$ 's was 100 or 200. In the continuum limit we find for the potential, using (1.9),

$$\exp(-2V(\varphi)) \sim \int_{-\infty}^{+\infty} \frac{\cos \varphi x}{|x|^{1/3}} dx \sim |\varphi|^{-2/3}. \quad (3.19)$$

The potential therefore has a logarithmic singularity in  $\varphi = 0$ :

$$V(\varphi) = J \log \frac{|\varphi|}{\pi}. \quad (3.20)$$

Such a singular potential falls outside the class considered by Ito<sup>5</sup>). An exact calculation of the partition function for this potential has not been made. Since, however, a similar logarithmic potential on a one-dimensional lattice gives rise to a sudden collapse into the saturated ferromagnetic state, when the temperature drops below a finite critical temperature<sup>10</sup>), it is very likely that the same phenomenon will occur for the potential of eq. (3.20) on a square lattice. We will not pursue this problem here.

We have not succeeded in finding more fixed points of the mapping of eq. (3.10). Therefore we now consider the linearised mapping in the neighbourhood of a point of the Gaussian line (3.11). Making again the continuum approximation and using the symmetry of the eigenfunction  $v(-x) = v(x)$ , the eigenvalue problem  $\tilde{M}_{ij} v_j = \lambda v_i$  becomes, with  $\tilde{M}_{ij}$  given by eq. (3.5),

$$4 \int_{-\infty}^{\infty} z(x) z^2(x+y) v(x) dx = \lambda v(y). \quad (3.21)$$

$v(x) = z(x)$  is an eigenfunction with eigenvalue  $\lambda = 4$ . For the original mapping this should be discarded, however. In order to calculate the remaining eigenvalues we substitute  $z(x)$  from eq. (3.11) into eq. (3.21) and obtain

$$\int_{-\infty}^{\infty} e^{-\frac{1}{2}(ax^2 + 2cxy + ay^2)} G_n(x) dx = \sigma_n G_n(y). \quad (3.22)$$

Here we have introduced the following abbreviations:

$$a = 5b; \quad c = 4b; \quad G_n(x) = e^{-\frac{1}{2}bx^2} v(x); \quad \sigma_n = \frac{\lambda_n}{4z_0^3}. \quad (3.23)$$

The general solution of eq. (3.22) is easily found to be<sup>11)</sup>

$$G_n(x) = H_n(\beta x) e^{-\frac{1}{2}dx^2} \quad \text{with} \quad \sigma_n = (-1)^n \sqrt{\frac{2\pi}{a+d}} \left( \frac{a-d}{a+d} \right)^{n/2}, \quad (3.24)$$

where

$$d = +\sqrt{a^2 - c^2} \quad \text{and} \quad \beta = \sqrt{d}. \quad (3.25)$$

This leads to  $\lambda_n = 4 \cdot (-\frac{1}{2})^n$ , but since only the Hermite polynomials  $H_n$  with even  $n$  are symmetric in  $x$ , the spectrum finally becomes

$$G(p): \quad \lambda_n = 4 \cdot \left(\frac{1}{4}\right)^n, \quad n = 0, 1, 2, \dots, \quad (3.26)$$

in agreement with the numerical result of eq. (1.18).

In a similar way we derive a continuum approximation for  $\text{RG}_2(0)$  by making the replacements  $z_{2m} \rightarrow z(x)$  and  $z_{2m+1} \rightarrow az(x)$ , which are suggested by the results of numerical calculations and are in agreement with the structure indicated in table I. In this way the equations for the fixed point of the mapping II (eq. (3.2)) become

$$z(y) = \frac{1}{2}(1 + a^4) \int_{-\infty}^{\infty} z^2(x) z^2(x+y) dx, \quad (3.27)$$

$$z(y) = a \int_{-\infty}^{\infty} z^2(x) z^2(x+y) dx.$$

From this we find for  $a$  the equation  $a^4 - 2a + 1 = 0$  (eq. (1.21)). With  $a = 1$  we recover  $G(0)$ . For the only other real solution  $a = 0.543689 \dots$  we obtain  $RG_2(0)$  with

$$z(x) = z_0 e^{-bx^2}, \quad z_0^3 = \frac{1}{a} \sqrt{\frac{4b}{\pi}}, \quad b \text{ arbitrary.} \quad (3.28)$$

If we substitute this continuum approximation into the matrix  $\tilde{M}_{ij}$  and also replace the eigenvectors by

$$\begin{pmatrix} v_{2j} \\ v_{2j+1} \end{pmatrix} \rightarrow \begin{pmatrix} f_0(x) \\ f_1(x) \end{pmatrix} = f(x) = f(-x), \quad (3.29)$$

the eigenvalue problem of the linearised mapping in a point  $RG_2(0)$  becomes

$$2 \int_{-\infty}^{\infty} z(x) z^2(x+y) A f(x) dx = \lambda f(y), \quad (3.30)$$

in which

$$A = \begin{pmatrix} 1 & a^3 \\ a^2 & a \end{pmatrix}. \quad (3.31)$$

The eigenvalues of  $A$  are

$$\mu_+ = 2a \quad \text{and} \quad \mu_- = 1 - a. \quad (3.32)$$

Let  $e_L^+$  be the corresponding left eigenvectors and  $h_{\pm}(x) = e_L^{\pm} \cdot f(x)$ . Eq. (3.30) then becomes

$$2\mu_{\pm} \int_{-\infty}^{\infty} z(x) z^2(x+y) h_{\pm}(x) dx = \lambda h_{\pm}(y), \quad (3.33)$$

which is again of the form of eq. (3.21). Considering only the even eigenfunctions, we find that the spectrum separates into a double series  $\lambda_n^{\pm} = (2\mu_{\pm}/a)(\frac{1}{4})^n$ , or

$$\lambda_n^+ = 4 \cdot (\frac{1}{4})^n \quad \text{and} \quad \lambda_n^- = 1.6785736 \cdot (\frac{1}{4})^n, \quad n = 0, 1, 2, \dots \quad (3.34)$$

In this way we have recovered the relevant eigenvalue  $\lambda_0^- = 1.6785736 \dots$ , which was given in table I.

The three-line solutions of table I can be obtained in the same way by making the replacements



$$z_{4m} \rightarrow z(x); \quad z_{4m \pm 1} \rightarrow a_1 z(x); \quad z_{4m \pm 2} \rightarrow a_2 z(x), \quad (3.35)$$

with again  $z(x) = z_0 e^{-bx^2}$ . The equations for  $a_1$  and  $a_2$  are

$$\begin{aligned} 1 + 2a_1^4 + a_2^4 &= 2a_1(1 + a_2^2), \\ a_2(1 + 2a_1^4 + a_2^4) &= 2(a_1^4 + a_2^2). \end{aligned} \quad (3.36)$$

For  $\text{RG}_3^{(1)}(0)$  we find  $a_1 = a$  and  $a_2 = a^2$  with  $a$  again satisfying eq. (1.21). For  $\text{RG}_3^{(2)}(0)$  we get  $a_1 = a_2 = a$ , with

$$3a^3 + a^2 + a - 1 = 0, \quad a = 0.4693964. \dots \quad (3.37)$$

These values of  $a$  agree perfectly with the values obtained numerically. The eigenvalue problem for the linearised mapping can be written as

$$\int_{-\infty}^{\infty} z(x) z^2(x+y) A f(x) dx = \lambda f(y); \quad f(-x) = f(x), \quad (3.38)$$

where the  $3 \times 3$  matrix  $A$  has the following form:

$$A_1 = \begin{pmatrix} 1 & 2a^3 & a^6 \\ a^2 & a(1+a^4) & a^4 \\ a^4 & 2a^3 & a^2 \end{pmatrix} \quad \text{for } \text{RG}_3^{(1)}(0)$$

and

$$A_2 = \begin{pmatrix} 1 & 2a^3 & a^3 \\ a^2 & a(1+a^2) & a^3 \\ a^2 & 2a^3 & a \end{pmatrix} \quad \text{for } \text{RG}_3^{(2)}(0).$$

The three eigenvalues of  $A_1$  are

$$\mu_0 = 4a^2; \quad \mu_+ = 2a(1-a); \quad \mu_- = (1-a)^2, \quad (3.39)$$

while those of  $A_2$  are

$$\mu_0 = 2a(1+a^2); \quad \mu_+ = 1-a; \quad \mu_- = a(1-a^2). \quad (3.40)$$

With each  $\mu_j$  a series in the spectrum of  $\tilde{M}$  can be associated, which is given by

$$\lambda_n^{(j)} = \frac{4\mu_j}{\mu_0} \left(\frac{1}{4}\right)^n, \quad n = 0, 1, 2, \dots \quad (3.41)$$

and where again the odd eigenfunctions had to be omitted. The series with  $j=0$  is the same as for  $G(0)$ . The value  $\lambda_0^{(0)}=4$  is absent in the original mapping, while the presence of  $\lambda_1^{(0)}=1$  indicates again that each point of  $\text{RG}_3^{(i)}(0)$  is an exact fixed point in the continuum limit. The remaining series begin with

$$\lambda_0^{(+)} = \frac{2(1-a)}{a} = 1.6785736 \dots \quad \text{and} \quad \lambda_0^{(-)} = \left( \frac{1-a}{a} \right)^2 = 0.70440 \dots$$

for  $\text{RG}_3^{(1)}(0)$  ,

(3.42)

$$\lambda_0^{(+)} = \frac{2(1-a)}{a(1+a^2)} = 1.8526018 \dots \quad \text{and} \quad \lambda_0^{(-)} = 2 \frac{1-a^2}{1+a^2} = 1.2777939 \dots$$

for  $\text{RG}_3^{(2)}(0)$  ,

again in perfect agreement with table I.

Using the same method all four-line structures of table II and the special five-line structures of table III were analysed. All eigenvalues, including their degeneracies, were verified.

The exact solution could also be given for the general case of  $N+1$  lines, of which  $N$  coincide. In the continuum approximation we make the replacements  $z_{2mN} \rightarrow z(x)$  and  $z_{2mN \pm j} \rightarrow az(x)$  for  $j=1, 2, \dots, N$ . The equations for the fixed point, which we denote by  $\text{RG}_{N+1}^{(d)}(0)$ , become

$$z(y) = \frac{1}{2N} (1 + (2N-1)a^4) \int_{-\infty}^{\infty} z^2(x) z^2(x+y) dx ,$$
(3.43)

$$az(y) = \frac{a^2}{N} (1 + (N-1)a^2) \int_{-\infty}^{\infty} z^2(x) z^2(x+y) dx .$$

This leads again to a solution  $z(x)$  of the form of eq. (3.28), with  $a$  given by the (unique) real positive solution of

$$(2N-1)a^3 + a^2 + a - 1 = 0 .$$
(3.44)

The eigenvalue problem of the linearised mapping in a point of  $\text{RG}_{N+1}^{(d)}(0)$  becomes  $\tilde{M}_{ij} v_j = \lambda v_i$ , which in the continuum approximation reads

$$\frac{2}{N} \int_{-\infty}^{\infty} z(x) z^2(x+y) A v(x) dx = \lambda v(y) .$$
(3.45)

The  $(N + 1)$ -dimensional matrix  $A$  is given by

$$A = \begin{pmatrix} 1 & \dots & \dots & \dots & a^3 \\ a^2 & a(1 + a^2) & & & \vdots \\ \vdots & & & a(1 + a^2) & a^3 \\ a^2 & \dots & \dots & \dots & a \end{pmatrix}, \quad (3.46)$$

where all off-diagonal elements except those in the first and in the last column are equal to  $2a^3$ . It has three different eigenvalues

$$\mu_0 = (1 - a^2)(1 + a); \quad \mu_d = a(1 - a^2); \quad \mu_N = 1 - a, \quad (3.47)$$

of which  $\mu_d$  is  $(N - 1)$ -fold degenerate. As for eq. (3.30) the eigenvalues  $\lambda$  of eq. (3.45) can now again be determined. There are three series

$$\lambda_n^{(j)} = 4 \frac{\mu_j}{\mu_0} \left(\frac{1}{4}\right)^n, \quad n = 0, 1, 2, \dots, \quad j = 0, d, N. \quad (3.48)$$

In the first series  $\lambda_n^{(0)} = 4, 1, \frac{1}{4}, \dots$  the value  $\lambda = 4$  must again be omitted. For the other two series we give the first term in table IV together with the value of

TABLE IV  
The spectrum and the values of  $a$  for the maximally degenerate  $(N + 1)$ -line solution.

$N$	$a$	$\lambda_0^{(d)}$ (degeneracy)	$\lambda_0^{(N)}$
1	0.5436890		1.6785735
2	0.4693964	1.2777938	1.8526016
3	0.4273046	1.1975149 ( 2×)	1.9634807
4	0.3984452	1.1396806 ( 3×)	2.0453568
5	0.3767544	1.0946161 ( 4×)	2.1103139
6	0.3595299	1.0578066 ( 5×)	2.1641255
7	0.3453389	1.0267716 ( 6×)	2.2100218
8	$\frac{1}{3}$	1 ( 7×)	$2\frac{1}{4}$
9	0.3229714	0.9765029 ( 8×)	2.2853836
10	0.3138869	0.9555979 ( 9×)	2.3170961
48	$\frac{1}{5}$	$\frac{2}{3}$ ( 47×)	$2\frac{7}{9}$
144	$\frac{1}{7}$	$\frac{1}{2}$ (143×)	$3\frac{1}{16}$

*a.* We notice that there is always at least one relevant eigenvalue and that the maximum number occurs for eight lines, i.e.,  $N = 7$ . The broken structure of fig. 5 has not yet been investigated in any detail.

However, we have found a multitude of other classes of fixed points. In fact we discovered that the number of (almost) fixed points of the mapping II (eq. (3.2)) is literally inexhaustible. This was seen when we tried to generalise the solutions of the form of eqs. (2.3) and (2.4) to

$$z_l = \tilde{z} \sum_i a_i e^{-b(l-\alpha i)^2}, \quad (3.49)$$

where the normalisation constant  $\tilde{z}$  will be chosen later and the summation over  $i$  runs from  $-\infty$  to  $+\infty$ . The peaks of which this function consists are well separated from each other when  $\alpha \gg 1/\sqrt{b}$ . In this case the square of  $z_l$  can be written as

$$z_l^2 \approx \tilde{z}^2 \sum_i a_i^2 e^{-2b(l-\alpha i)^2}. \quad (3.50)$$

These two expressions should be substituted into the equation for the fixed point  $z_l = \sum_m z_m^2 z_{m+l}^2$ . When again  $l$  and  $m$  are replaced by the continuous variables  $y$  and  $x$  and the integration over  $x$  is performed, we get

$$\tilde{z} \sum_i a_i e^{-b(y-\alpha i)^2} = \tilde{z}^4 \left( \frac{\pi}{4b} \right)^{1/2} \sum_{j,k} a_j^2 a_k^2 e^{-b(y-\alpha(k-j))^2}. \quad (3.51)$$

If we take  $\tilde{z}^3 = (4b/\pi)^{1/2}$  this equation is an identity in  $y$ , provided  $a_i$  is a solution of the equations

$$a_i = \sum_j a_j^2 a_{j+1}^2. \quad (3.52)$$

This is exactly the fixed point equation of the original mapping of eq. (1.11).

When we linearise the mapping in such a new fixed point, every eigenvalue is the product of two eigenvalues, one belonging to  $G(0)$  and the other to the (almost) fixed point we choose as a solution of eq. (3.52). If also for this the solution  $G(0)$  is chosen, we get the solution (2.3) and the spectrum is given by

$$\lambda_k = 4\left(\frac{1}{4}\right)^k \quad \text{with } (2k+1)\text{-fold degeneracy}. \quad (3.53)$$

If we choose  $RG_2(0)$  as the fixed point of eq. (3.52), we get the solution (2.4) and the spectrum consists of two series, the first again being given by eq. (3.53), the second by

$$\tilde{\lambda}_k = c(\frac{1}{4})^k; \quad c = \frac{2(1-a)}{a} \\ = 1.6785736 \dots \quad \text{with } (2k+1)\text{-fold degeneracy.} \quad (3.54)$$

In both cases  $\lambda = 1$  is three-fold degenerate, which is in agreement with the fact that the fixed points are characterised by three continuous parameters. These solutions with  $G(0)$  and with  $RG_2(0)$  have been confirmed numerically.

Since the subject of fixed points is really inexhaustible we will not dwell on it any longer, but turn our attention to the potentials belonging to these fixed points and to the related phase transitions. This will be discussed in the next section.

#### 4. Potentials and phase diagrams

When the Migdal transformation (1.4)–(1.11) is applied repeatedly, starting from an arbitrary potential  $V(\varphi)$  with  $V(0) = 0$ , the generated potentials will approach a limiting function  $V^*(\varphi)$ , which is related to some fixed point  $u^*$  of  $I$ , eq. (3.1), by eq. (3.7). The domains of attraction of these fixed points are separated by the stable manifolds of the relevant fixed points. For an arbitrary potential – which changes when we vary the temperature and the coupling constants – we can get an idea of the equilibrium phase of the system by determining the ground state of the fixed point potential  $V^*(\varphi)$ , by which it is attracted under the Migdal transformation. Finding this ground state may be quite difficult, but a picture of the potential often suffices to give an indication of the phase.

The attractive fixed points are the trivial point  $T$  with  $V_T^*(\varphi) \equiv 0$  and the points belonging to the classes  $G(p)$  and  $SG(p)$ . All other fixed points have a largest eigenvalue greater than one.

In fig. 6 we have plotted two of these attractive potentials belonging to  $G(0)$  and  $G(1)$ . It is also shown how these limiting potentials were approached when the starting potential was close to the relevant fixed point  $RG_2(0)$ . Also for the degenerate states  $RG_{N+1}^{(d)}(0)$ , cf. eq. (3.43), the potential  $V_N^{(d)}(\varphi)$  can be calculated from eq. (3.7). Using Poisson's formula we obtain

$$\exp(-2V_N^{(d)}(\varphi)) = f \sum_n \left[ 2Na \exp\left(-\frac{(\varphi - 2\pi n)^2}{4b}\right) \right. \\ \left. + (1-a) \exp\left(-\frac{(\varphi - \pi n/N)^2}{4b}\right) \right], \quad (4.1)$$

where the normalisation factor is fixed by requiring  $V_N^{(d)}(0) = 0$  and  $a$  can be

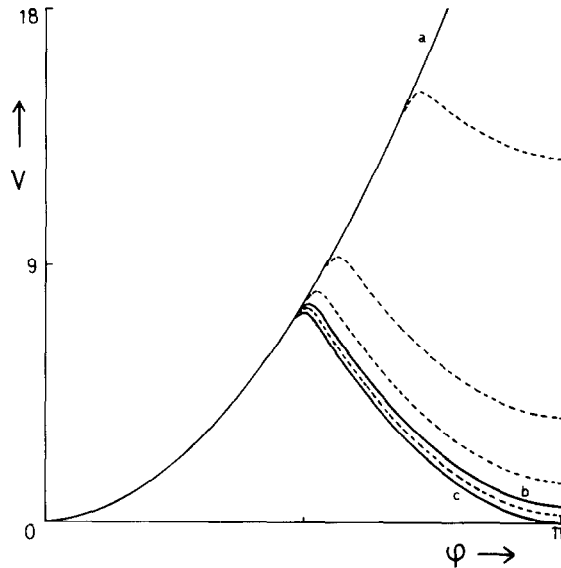


Fig. 6. The potentials belonging to  $G(0)$ ,  $RG_2(0)$  and  $G(1)$ , represented by, respectively, a, b and c. The dashed lines show intermediate potentials when  $G(0)$  or  $G(1)$  is approached starting from the unstable fixed point  $RG_2(0)$ .

read from table IV. For  $N=4$  and  $N=8$  these potentials were calculated numerically. They are shown in figs. 7a and 7b. In the same way we calculated the potential belonging to the fixed point of the type  $SG(0)$ , described by eq. (2.3). For two sets of values of  $\alpha$ ,  $b$  and  $\gamma$  the results are plotted in fig. 8. Both cases correspond to fixed points, which were found numerically.

The appearance of high maxima in the fixed point potentials of Gaussian-type indicates that they correspond to thermodynamic phases which may be very different from each other. A flow diagram showing the separation between these phases may be obtained by determining, for each unstable fixed point potential, into which stable potential it decays under the mapping. For the relevant structures of tables I–IV the corresponding stable structures are obtained by shifting one or more lines either to the top line or down to infinity. The latter operation amounts to inserting zeroes for certain  $\mu_i$ 's. Not all possibilities are allowed however, the remaining point must be a fixed point of (4.2). More complicated flow diagrams can be obtained by considering the mapping for a general  $N+1$ -line solution. There are  $N$  different  $a$ 's which transform under the mapping as

$$a'_1 = 2 \left( 1 + a_N^4 + 2 \sum_{k=1}^{N-1} a_k^4 \right)^{-1} \sum_{k=0}^{N-1} a_k^2 a_{k+1}^2, \quad (4.2)$$

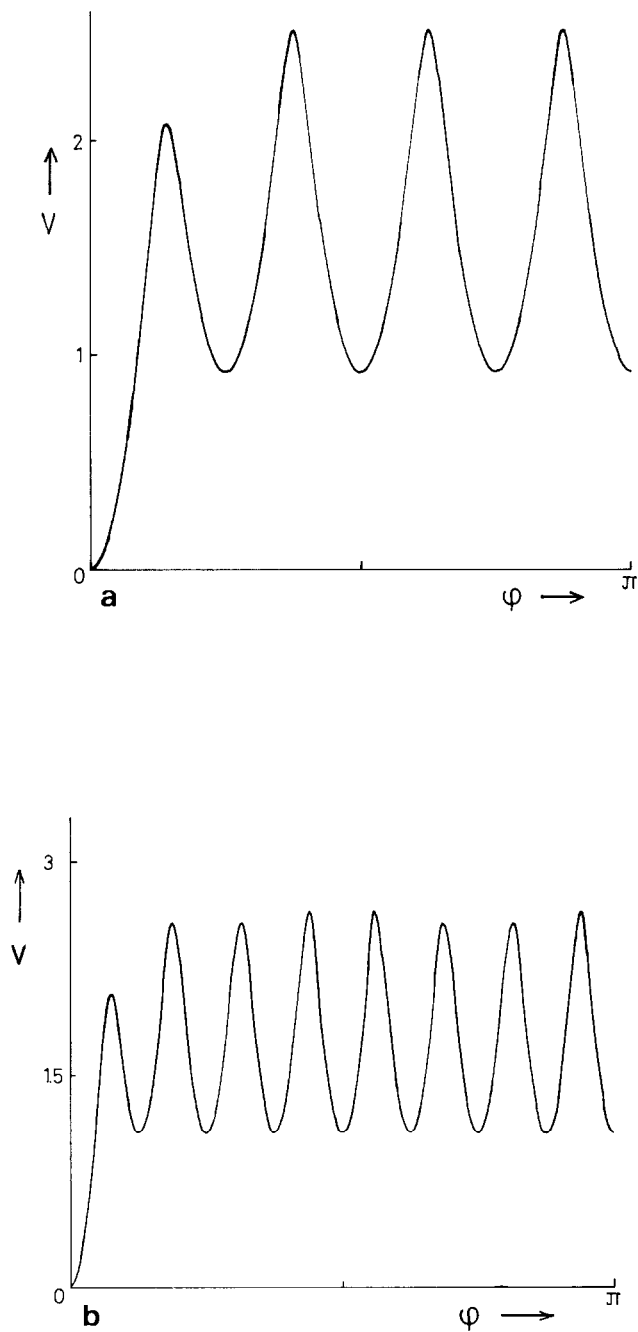


Fig. 7. The potentials for the maximally degenerate line solutions (4.1) for two cases. (a)  $N = 4$ . (b)  $N = 8$ .

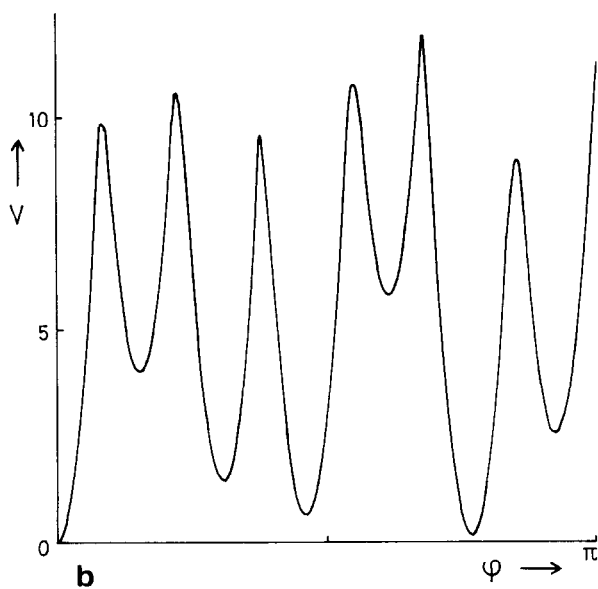
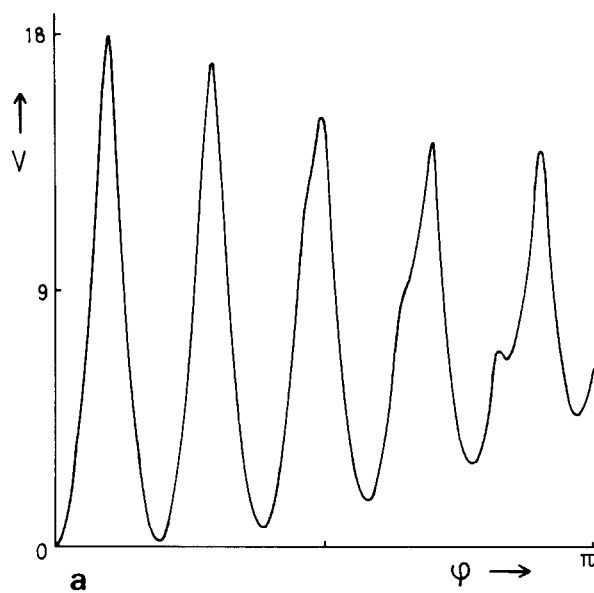


Fig. 8. The potentials of three-dimensional fixed space, described by (2.3), for two sets of parameters. (a)  $\alpha = 10.3$ ,  $b = 0.25$ ,  $\gamma = 0.07$ . (b)  $\alpha = 2.6$ ,  $b = 4.5$ ,  $\gamma = 0.01$ .



with  $a_0 = 1$ ,  $a_{N+k} = a_{N-k}$  and  $a_{2N+k} = a_k$ . For the case  $N = 2$  the resulting flow diagram is shown in fig. 9. If in ref. 2 the limit  $\gamma \rightarrow 1$  is taken, our picture is equal to fig. 6 there.

Another way to study the phase diagram is to take an interparticle potential of a fixed form, but containing one or more parameters. For each parameter set it is then determined into which stable fixed point this potential is transformed by a large number of Migdal transformations. In this way the parameter space of the chosen potential is divided into regions inside each of which the thermodynamic state is the same. For a number of two-parameter potentials we have applied this procedure. The resulting phase boundaries are shown in figs. 10 and 11. Fig. 10 gives the phase diagram for the potential

$$V(\varphi) = B \cos^2(7\varphi) + C\varphi^2. \quad (4.3)$$

It is an example of a case in which for some values of the parameters  $B$  and  $C$  the potential is mapped into a function of the type shown in fig. 8 and belonging to a three-dimensional subset of fixed points. We will not speculate about the thermodynamic phase belonging to such a potential.

Figs. 11a and 11b give the phase diagram for the potential

$$V(\varphi) = -B \cos \varphi + C \cos^2 \varphi. \quad (4.4)$$

For each of the three regions we have indicated whether an initial potential in that region approaches  $G(0)$ ,  $G(1)$  or  $T$ , i.e., the trivial (high temperature) point. The diagram 11b is of the same form as derived in refs. 1 and 2. The phase boundaries between  $T$  and  $G(0)$  and between  $T$  and  $G(1)$  describe the Kosterlitz–Thouless transition, whereas the  $G(0)$ – $G(1)$  boundary is said to be of Ising-type<sup>1</sup>). However, a number of remarks are in order. Since the work of

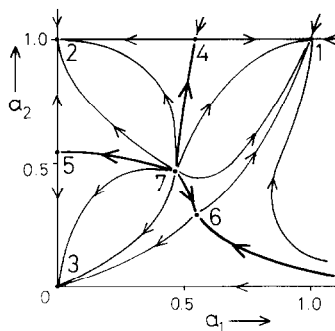


Fig. 9. The flow diagram for the mapping (4.2) with  $N = 2$ , which contains all three-line solutions.

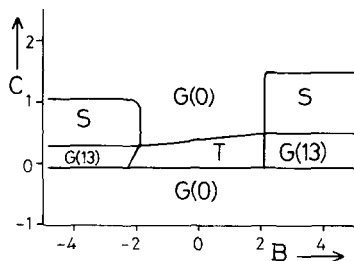


Fig. 10. Phase diagram for the potential  $V(\varphi) = B \cos^2(7\varphi) + C\varphi^2$  (eq. (4.3)).

ref. 6 it is known that a calculation of the Kosterlitz–Thouless phase boundary, using the Migdal approximation, can at most give an indication of its existence. The same situation arises here, because the position of the boundary depends on whether we use single or double precision in our computer calculations.

The  $G(0)$ – $G(1)$  transition does not depend on such subtleties. Still the question remains whether the Migdal approximation describes it well. In order to decide this question we have compared our calculations with those of Lee and Grinstein<sup>1</sup>). For  $C < 0$  they approximate the potential (4.4) by an expression derived from

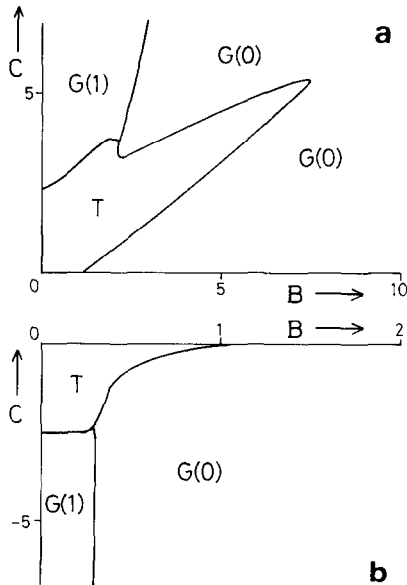


Fig. 11. Phase diagram for the potential  $V(\varphi) = -B \cos \varphi + C \cos^2 \varphi$  (eq. (4.4)). (a) Positive  $C$ , (b) negative  $C$ .

$$e^{-2V(\varphi)} \sim \sum_n \{ \exp[-\frac{1}{2}K(\varphi - 2\pi n)^2] + \exp[-\Gamma - \frac{1}{2}K(\varphi - \pi - 2\pi n)^2] \} , \quad (4.5)$$

which is a modified Villain model. This potential is exactly equal to our potential for the fixed point  $RG_2(0)$  and given by eq. (4.1) with  $N = 1$  and the further correspondence

$$K = \frac{1}{2b} \quad \text{and} \quad e^{-\Gamma} = \frac{1-a}{1+a} . \quad (4.6)$$

For the critical value of  $a$  we obtained  $a = 0.5436890$  (see table IV), corresponding to  $\Gamma_{cr} = 1.2187$ . We found this value to be independent of  $b$ , i.e., independent of  $K$ . Without making the Migdal approximation, Lee and Grinstein derive the following relation between  $\Gamma$  and  $K_I$ , with  $K_I$  the coupling constant of the two-dimensional Ising model, which they show to be equivalent to their potential:

$$e^{-\Gamma} = \tanh K_I . \quad (4.7)$$

Combining (4.6) and (4.7) we find

$$K_I = -\frac{1}{2} \ln a . \quad (4.8)$$

Now we will show that the Migdal approximation gives the same result for the  $RG_2$  transition for continuous spins as for the two-dimensional Ising model. Using (4.8) it can be seen that the fixed-point equation for  $K_I$  in the Migdal approximation<sup>13</sup>:

$$K_I = \frac{1}{2} \ln \cosh 4K_I \quad (4.9)$$

gives for  $a$  the equation  $a^4 - 2a + 1 = 0$ , which is eq. (1.21). The solution of this equation is  $a_{cr} = 0.543689 \dots$  which gives  $K_{Icr} = 0.30469 \dots$  (The exact value is  $K_{Icr} = -\frac{1}{2} \ln(\sqrt{2} - 1) = 0.44069 \dots$ ) Also the critical exponent  $\nu$ , defined by  $\nu = \ln 2 / \ln |\lambda_{\max}|$ , for the  $RG_2$  transition is exactly the same as the one for the Ising model. Some other relevant line solutions correspond to  $q$ -state Potts model transitions. In the following tables (V and VI) we compare the critical temperature  $K_{Icr}$  and exponent  $\nu$  for the  $q$ -state Potts model (including the Ising model) and for the continuous spins, both in the Migdal approximation. We have assumed (4.8) to hold also for the Potts model, although it is only derived for the Ising case. Although the numerical values for

TABLE V  
Critical couplings in the Migdal approximation for the  $q$ -state Potts model and for continuous spins.

$q$	$K_{\text{cr}}^*$	Solution	$K_{\text{cr}}^{**}$	$a_{\text{cr}}$
2	0.305	$\text{RG}_2$	0.3047	0.54369
3	0.347	$\text{RG}_4^{(3)}$	0.3466	0.50000
4	0.378	$\text{RG}_3^{(2)}$	0.3782	0.46939

\*These values for the  $q$ -state Potts model are from ref. 14, table I.

\*\*Our results, assuming the relation  $K_1 = -\frac{1}{2} \ln a$ .

critical couplings and exponents in the Migdal approximation differ considerably from the exact results<sup>14</sup>), it turns out there is exact agreement between transitions for continuous spins and those of the  $q$ -state Potts model (which as a special case contains the Ising model.) Our results are therefore in agreement with those of Lee and Grinstein<sup>1</sup>) and extend them. These remarks refer to fig. 11b in which  $C < 0$ . (We only consider  $B > 0$ , since the phase diagram is symmetric under  $B \rightarrow -B$ . This is a consequence of the form of the mapping.) For  $C > 0$  the potential (4.4) has its minima no longer at the boundary but rather inside the interval  $(-\pi, \pi)$ . Therefore it can no longer be approximated by a potential of the form (4.5). Instead Lee, Grinstein and Toner<sup>1</sup>) choose another Villain-type approximation for which they make the hypothesis that it gives the same set of phases and universality classes. Of the five phases which they find only three, viz. the paramagnetic (PM), the ferromagnetic (FM) and the staggered nematic (SN), are recovered in the Migdal approximation. In fig. 11a they are indicated by the names of the corresponding fixed points T, G(0) and G(1) (nematic instead of staggered nematic), respectively. The other two phases, "ICE" and staggered triatic (ST) do not occur in the Migdal approximation.

TABLE VI  
Critical exponents in the Migdal approximation for the  $q$ -state Potts model and for the continuous spins.

$q$	$1/\nu^*$	Solution	$1/\nu^{**}$	$\lambda_{\text{max}}$
2	0.747	$\text{RG}_2$	0.7472	1.6785
3	0.830	$\text{RG}_4^{(3)}$	0.8301	1.7777
4	0.890	$\text{RG}_3^{(2)}$	0.8896	1.8526

\*These values of  $1/\nu = y_i$  for the  $q$ -state Potts model are from ref. 14, table I.

\*\*Our results for continuous spins with  $\nu = \ln 2 / \ln |\lambda_{\text{max}}|$ .

## 5. Conclusions

For a system of two-dimensional spins on a square lattice, with an arbitrary but only nearest neighbour interaction, the problem of finding all possible phase transitions and of calculating the critical temperatures and critical exponents is a formidable one. Even the less ambitious task of sketching the phase diagram for any given interaction has only met with partial success. Examples are given in the work of Kosterlitz and Thouless<sup>12)</sup> and in refs. 1–9.

If, however, Migdal's bond-moving method is used as an approximation, the problem becomes tractable, as was shown in the previous sections. Our conclusions, describing the advantages and the short-comings of the Migdal approximation, may be summarised in the following points.

1) We found numerically a new denumerable set of unstable almost fixed lines, by generalisation of an earlier found set of stable almost fixed lines. We also found a new stable and unstable three-dimensional almost fixed space. By making a continuum approximation we analytically constructed all numerically found fixed points and the transformations to construct new ones.

2) Given an (almost) fixed point  $Y$  of (1.11) a new one can be constructed in three ways:

a) by inserting a fixed number ( $p$ ) of zero's between each pair of consecutive  $\mu_i$ 's<sup>4)</sup> ( $Y(0) \rightarrow Y(p)$ ):

$$\tilde{\mu} = \begin{cases} \mu_{l/p} & \text{if } l/p \text{ is integer,} \\ 0 & \text{otherwise.} \end{cases}$$

b) By using (3.49) and (3.52), the dimension of the fixed space will be increased by two ( $Y \rightarrow SY$ ):

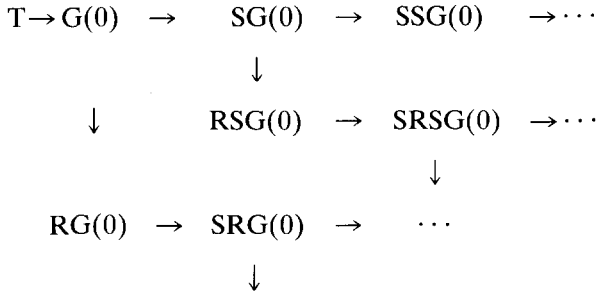
$$\tilde{\mu}_l = \sum_i \mu_i e^{-b(l-i\alpha)^2}.$$

c) By making a multi-line solution, which is only possible if the original (almost) fixed point  $\mu_i$  satisfies the continuum equation (3.10) ( $Y \rightarrow RY$ ):

$$\tilde{\mu}_{2Nj+i} = a_i \cdot \mu_{2Nj+i}; \quad i = 0, 1, \dots, 2N-1, \quad j = \dots, -1, 0, 1, \dots,$$

with  $a_0 = 1$ ,  $a_{2N-j} = a_j$ ,  $a_{2N+j} = a_j$  and the  $a_i$ 's satisfying (4.2).

3) Starting from the exact fixed point  $T(\mu_i = \delta_{i0})$  we can construct an infinite hierarchy of (almost) fixed points, as is partly shown in the scheme below [horizontally we apply b), vertically c), a) is not shown]:



Each fixed space in the hierarchy can be described by a list of R's and S's, describing how it was constructed starting from T, and the number of zeroes between the  $\mu$ 's. It is not allowed to apply R two consecutive times, because a multi-line solution does not satisfy (3.10). The transformations a) and c) commute and  $SY(p)$  is the same as  $SY(0)$  with a different  $\alpha$ .

4) We have confirmed previous findings<sup>6)</sup> in that the almost fixed points are not absolutely invariant under the Migdal transformation, but only within the computer accuracy. They become exactly fixed points in the zero-temperature limit. In this limit the potential is singular and different from the trivial (high temperature) one.

5) Using the continuum approximation we have calculated the spectrum of the almost fixed points. In a given almost fixed space the eigenvalues are the same for all points. The agreement with the numerical results was striking. We have shown that the phase transitions described by some of the relevant fixed lines are Ising-like in the sense that the Migdal renormalisation gives the same critical exponents (and temperatures) for these transitions as for the ones of the  $q$ -state Potts model. (They differ considerably from the exact values.)

In the Migdal approximation no quantitative predictions can be made for the Kosterlitz–Thouless transitions, because the almost fixed lines have no well-defined end points, as was already shown by Jose et al.<sup>6)</sup>

6) For a few fixed points the corresponding potential has been calculated. For some two-parameter potentials the phase diagram is constructed and is compared with the ones obtained by other methods. The results suggest that the Migdal approximation gives a reasonable picture of the phase diagram, including the character of the different phases.

## Acknowledgements

We would like to thank Dr. J. van Himbergen and Dr. H. van Beijeren for stimulating and fruitful discussions. One of us (K.S.) acknowledges the finan-

cial support from the “Stichting F.O.M.”, which is funded by the “Nederlandse Organisatie voor Zuiver-Wetenschappelijk Onderzoek (Z.W.O.)”.

## References

- 1) D.H. Lee and G. Grinstein, Phys. Rev. Lett. **55** (1985) 541.  
See also D.H. Lee, G. Grinstein and J. Toner, Phys. Rev. Lett. **56** (1986) 2318.
- 2) S.E. Korshunov, J. Phys. C: Solid State Phys. **19** (1986) 4427.
- 3) A.A. Migdal, Sov. Phys. JETP **42** (1976) 743.
- 4) K. Sokalski and Th. W. Ruijgrok, Physica **130A** (1985) 412.
- 5) K.R. Ito, Phys. Rev. Lett. **54** (1985) 2383.
- 6) J.V. José, L.P. Kadanoff, S. Kirkpatrick and D.R. Nelson, Phys. Rev. B **16** (1977) 1217.
- 7) J. Fröhlich and T. Spencer, Commun. Math. Phys. **81** (1981) 527.
- 8) J. Villain, J. Phys. (Paris) **36** (1975) 581. See also ref. 6, section IIIB.
- 9) H.J.F. Knops, in: Fundamental Problems in Statistical Mechanics V, E.G.D. Cohen, ed. (1980).
- 10) Th. Niemcijsz and Th. W. Ruijgrok, Physica **86A** (1977) 200.
- 11) I.S. Gradshteyn and I.M. Ryzhik, Table of Integrals, Series, and Products (Academic, New York, 1965), eq. 7.374.8.
- 12) J.M. Kosterlitz and D.J. Thouless, J. Phys. C: Solid State Phys. **6** (1973) 1181.  
J.M. Kosterlitz, J. Phys. C: Solid State Phys. **7** (1974) 1046.
- 13) S. Caracciolo, Nucl. Phys. B **180** (1981) 405.
- 14) H.H. Chen, Felix Lee and H.C. Tseng, Phys. Rev. B **34** (1986) 6448.